THE JOURNAL OF PHYSICAL CHEMISTRY Letters

Cite This: J. Phys. Chem. Lett. 2018, 9, 6517−6523

Letter

pubs.acs.org/JPCL

Role of H Transfer in the Gas-Phase Sulfidation Process of MoO_3: A Quantum Molecular Dynamics Study

Chunyang Sheng,[†,⊥] Sungwook Hong,[†,⊥] Aravind Krishnamoorthy,[†] Rajiv K. Kalia,[†] Aiichiro Nakano,[†] Fuyuki Shimojo,[‡] and Priya Vashishta*[,†]

[†]Collaboratory for Advanced Computing and Simulations, Department of Chemical Engineering & Materials Science, Department of Physics & Astronomy, Department of Computer Science, and Department of Biological Sciences, University of Southern California, Los Angeles, California 90089-0242, United States

[‡]Department of Physics, Kumamoto University, Kumamoto 860-8555, Japan

Supporting Information

ABSTRACT: Layered transition metal dichalcogenide (TMDC) materials have received great attention because of their remarkable electronic, optical, and chemical properties. Among typical TMDC family members, monolayer MoS_2 has been considered a next-generation semiconducting material, primarily due to a higher carrier mobility and larger band gap. The key enabler to bring such a promising MoS_2 layer into mass production is chemical vapor deposition (CVD). During CVD synthesis, gas-phase sulfidation of MoO_3 is a key elementary reaction, forming MoS_2 layers on a target substrate. Recent studies have proposed the use of gas-phase H_2S precursors instead of condensed-phase sulfur for the synthesis of higher-quality MoS_2 crystals. However, reaction mechanisms, including atomic-level reaction pathways, are unknown for MoO_3 sulfidation by H_2S. Here, we report first-principles quantum molecular dynamics (QMD) simulations to investigate gas-phase sulfidation of MoO_3 flake using a H_2S precursor. Our QMD results reveal that gas-phase H_2S molecules efficiently reduce and sulfidize MoO_3 through the following reaction steps: Initially, H transfer occurs from the H_2S molecule to low molecular weight Mo_xO_y clusters, sublimated from the MoO_3 flake, leading to the formation of molybdenum oxyhydride clusters as reaction intermediates. Next, two neighboring hydroxyl groups on the oxyhydride cluster preferentially react with each other, forming water molecules. The oxygen vacancy formed on the Mo−O−H cluster as a result of this dehydration reaction becomes the reaction site for subsequent sulfidation by H_2S that results in the formation of stable Mo−S bonds. The identification of this reaction pathway and Mo−O and Mo−O−H reaction intermediates from unbiased QMD simulations may be utilized to construct reactive force fields (ReaxFF) for multimillion-atom reactive MD simulations.

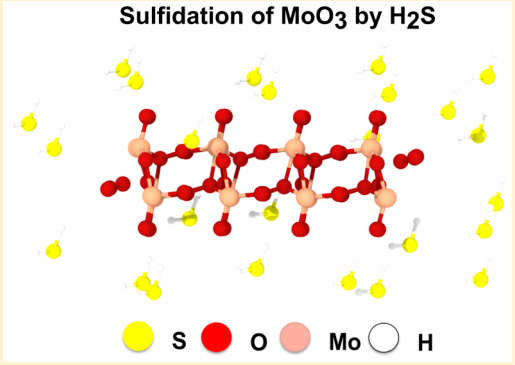

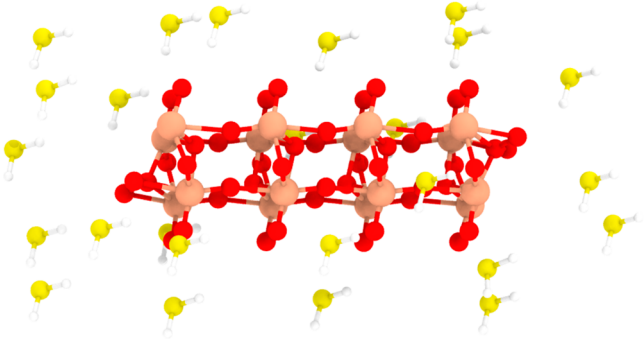

Figure 1. Initial configuration of MoO_3/H_2S: a monolayered MoO_3 flake is placed in the middle of the simulation domain surrounded by 25 H_2S molecules. The MoO_3 flake contains fully O-terminated sites, consistent with experimental conditions (pink: Mo atoms; red: O atoms; yellow: S atoms; white: H atoms).

Two-dimensional materials like graphene and transition metal dichalcogenides (TMDCs) have led to the exploration of novel nanostructures with remarkable functionality.[1−5] In particular, monolayer molybdenum disulfide (MoS_2), an archetypal layered TMDC material, has attracted great attention due to its large direct band gap, high carrier mobility, excellent current on/off ratio, and interesting photoluminescence features as well as exceptional mechanical properties.[6−12] Monolayer MoS_2 is also considered an outstanding candidate for a wide range of nanoscale applications such as single-layer MoS_2 transistors,[13−15] ultrasensitive photodetectors,[10] monolayered heterojunction solar cells,[7] MoS_2-supported gold nanoparticles for methanol synthesis,[16] and catalysts for the electrochemical hydrogen evolution reaction.[17] Among different types of synthesis

Received: July 9, 2018
Accepted: October 8, 2018
Published: October 8, 2018

DOI: 10.1021/acs.jpclett.8b02151
J. Phys. Chem. Lett. 2018, 9, 6517−6523

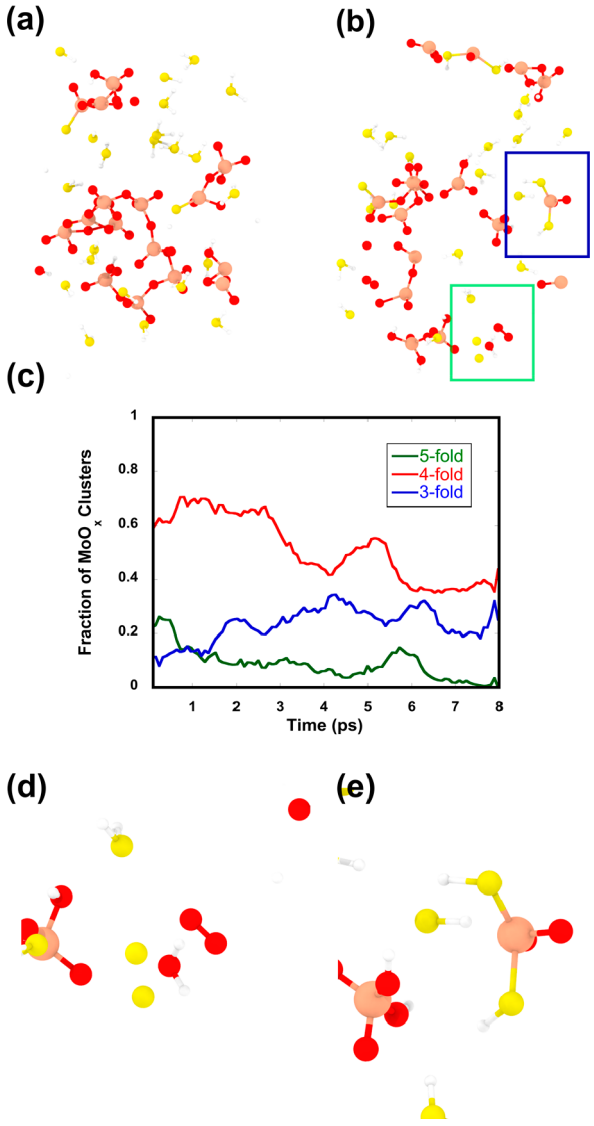

Figure 2. QMD snapshots of the gas-phase sulfidation processes at (a) 1.3 and (b) 4.2 ps, respectively. The initial MoO_3 flake ejects $Mo_xO_{y\,(x=2,3)}$ clusters at 2500 K (c). Changes in Mo coordination numbers on $Mo_xO_{y\,(x=2,3)}$ clusters during the sulfidation process (d,e). Inset images in (b) show the formation of water (the green rectangle) and the Mo−S bond (the blue rectangle), respectively.

techniques for MoS_2 layers such as mechanical exfoliation, physical vapor deposition, and chemical vapor deposition (CVD).[18−20] CVD is the most practical method for growing controllable large-area MoS_2 layers because of its scalability and the uniformity and stability of grown films.[21−25] A typical CVD setup for synthesis of monolayer MoS_2 includes a carrier gas flowing in one direction, a certain amount of sulfur powder upstream of the gas flow, a certain amount of MoO_3 powder in the midstream, and a substrate for MoS_2 growth placed either on top of MoO_3 powder or next to it downstream. During CVD synthesis, a reaction chamber is usually heated above 1000 K, and Ar or N_2 are generally used as carrier gases. At such high temperatures, sulfur powder starts evaporating and reduces MoO_3 to volatile MoO_{3-x} suboxide. Sublimated Mo_xO_y suboxide clusters in turn diffuse toward the substrate and further react with gas-phase sulfur, forming MoS_2 fragments that are deposited on the substrate as a monolayer.[6,24−26] Extensive experimental studies have been conducted to understand the sulfidation processes of MoO_3 reactants with sulfur precursors.[22,23,27,28] The basic steps of the MoO_3 sulfidation processes were proposed using X-ray photoelectron and infrared emission spectroscopy experiments,[27] and it was inferred that the exchange of S atoms in the sulfur precursor with O atoms in MoO_3 reactants is the key reaction step for the sulfidation process. Furthermore, recent studies proposed that continuity and uniformity of MoS_2 layers could be improved by the proper selection of sulfur precursor. Namely, gas-phase H_2S precursor, instead of the conventional sulfur powder, could lead to the synthesis of high-quality monolayer MoS_2.[13,15]

However, atomic-level reaction pathways for the sulfidation process of the MoO_3 reactants have remained unclear because of the short length and time scales involved, which are beyond the spatial and temporal resolution of experimental techniques. To provide a better understanding of the sulfidation process of MoO_3, the main scientific questions are (1) what are the reaction pathways of the sulfidation process using MoO_3 reactants and H_2S precursors and (2) what is the role of hydrogen in these reaction pathways. To address these questions, we perform first-principles quantum molecular dynamics (QMD) simulations based on the density functional theory (DFT)[29,30] that provide unbiased information about the detailed atomistic pathways for the sulfidation of MoO_3 flake by H_2S. In the following, we provide computational details of QMD simulations, followed by results and discussion and conclusions of this study.

In this work, we used highly parallelized QMD simulation software developed by the authors.[31] During QMD simulations, electronic states were calculated using the projector-augmented wave (PAW) method.[32] Projector functions were generated for the 2s and 2p states of O atoms, the 1s state for H, the 3s and 3p of S atoms, and the 3d, 4s, and 4p states of Mo atoms. The generalized gradient approximation[33] was used for the exchange−correlation energy with nonlinear core corrections.[31] The DFT-D method was employed for semi-empirical correction of the van der Waals interaction.[34] In order to assess the effects of spin polarization and on-site Coulomb interaction between localized d-electrons, spin-polarized DFT and DFT+U calculations were employed, but they were found not to change key findings.[35] The momentum-space formalism was utilized, where the plane-wave cutoff energies were set to be 40 and 250 Ry for the electronic pseudowave functions and the pseudocharge density, respectively. The energy functional was minimized iteratively using a preconditioned conjugate-gradient method. In these simulations, a pair of atoms is considered to be bonded if their interatomic distances in the simulation cell are less than the cutoff distance for the given pair of elements. These cutoff distances are chosen from bond lengths available in experimental literature.[36−38] Further, these bonds are considered to be stable if the lifetime of the bond is greater than 10 fs. The initial configuration for our QMD simulations consists of a full monolayered MoO_3 flake (i.e., fully O-terminated MoO_3 surface) consisting of 16 MoO_3 formula units (representative of MoO_3 powder used in CVD)[39,40] and 25 H_2S molecules in an orthogonal supercell (22.185 Å × 14.302 Å × 19.120 Å) with periodic boundary conditions along *x*-, *y*-, and *z*-directions. This initial configuration (Figure 1) is initially relaxed using the quasi-Newton method[41] to

DOI: 10.1021/acs.jpclett.8b02151
J. Phys. Chem. Lett. 2018, 9, 6517−6523

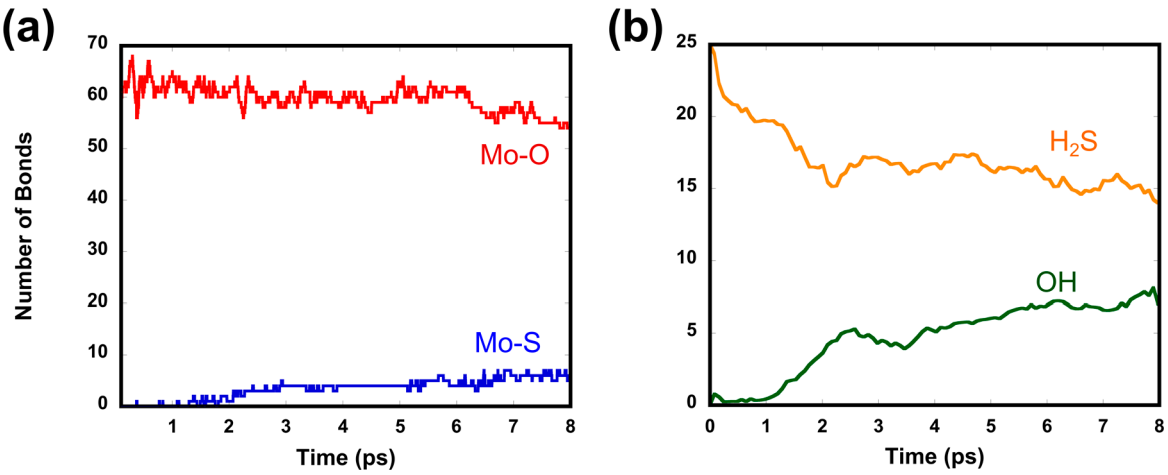

Figure 3. (a) Time evolution of Mo−O (red) and Mo−S bonds (blue). As time elapses, the number of the Mo−O bond decreases as the water molecules form while the Mo−S bond decreases, indicating that the formation of the water molecule is primarily responsible for Mo−S bond formation; (b) time evolution of H_2S molecular species and OH species on the $Mo_xO_{y\,(x=2,3)}$ clusters.

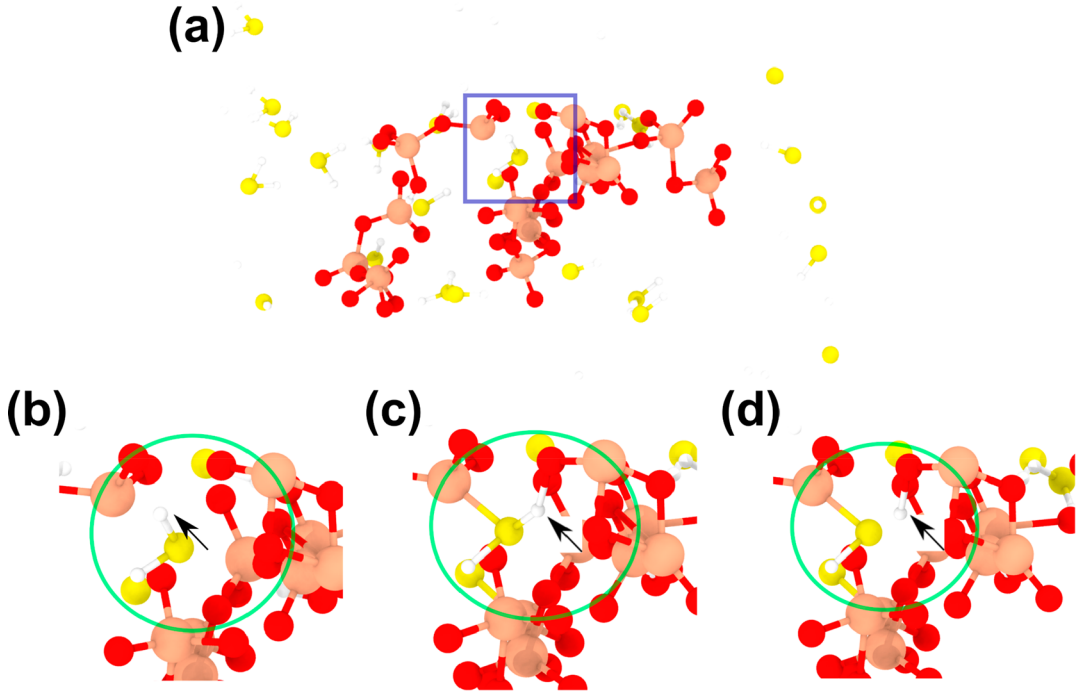

Figure 4. Reaction pathways for the initial H transfer and Mo−S bond formation: (a) overall system snapshot at 1.970 ps. (b−d) Inset images of the blue solid rectangle in (a); (b) at 1.970 ps; (c) at 1.985 ps; and (d) at 1.986 ps. Green circles in (b−d) highlight the key reaction events that include the H transfer and Mo−S bond formation, and black arrows point to the H atom participating in H transfer from the H_2S molecule to the ejected $Mo_xO_{y\,(x=2,3)}$ cluster.

remove residual forces and then used to perform QMD simulations.

QMD simulations are performed using the *NVT* ensemble (i.e., the average temperature, simulation cell dimensions, and number of particles are kept constant throughout the simulations), where a Nosé−Hoover thermostat[42,43] is used to maintain the temperature of the simulated system at 2500 K. Quantum-mechanically computed equations of motion for all atoms are integrated with a time step of 0.85 fs over an 8 ps long trajectory. QMD simulations are performed at an elevated temperature of 2500 K (compared to the experimental growth temperature of ∼1500 K[21,25]) in order to increase collision rates and thus observe important pathways and reaction steps within the very brief time window (∼8 ps) that can be investigated in QMD simulations.

Figure 2a,b depicts snapshots of the simulation cell at 1.3 and 4.2 ps after the beginning of the QMD simulation. The MoO_3 flake ejects several $Mo_xO_{y\,(x=2,3)}$ fragments of varying molecular weights, including transient MoO_4 clusters, that are stable for only ∼0.2 ps. Such unstable clusters quickly agglomerate with other sublimated MoO_x fragments to form larger $Mo_xO_{y\,(x=2,3)}$ clusters. These clusters, predominantly Mo_2O_7 (average lifetime of >10.4 ps), are the main reaction intermediates that undergo both reduction and sulfidation reactions with H_2S. This is accompanied by a change in the local coordination number of Mo ions from the six-fold

DOI: 10.1021/acs.jpclett.8b02151
J. Phys. Chem. Lett. 2018, 9, 6517−6523

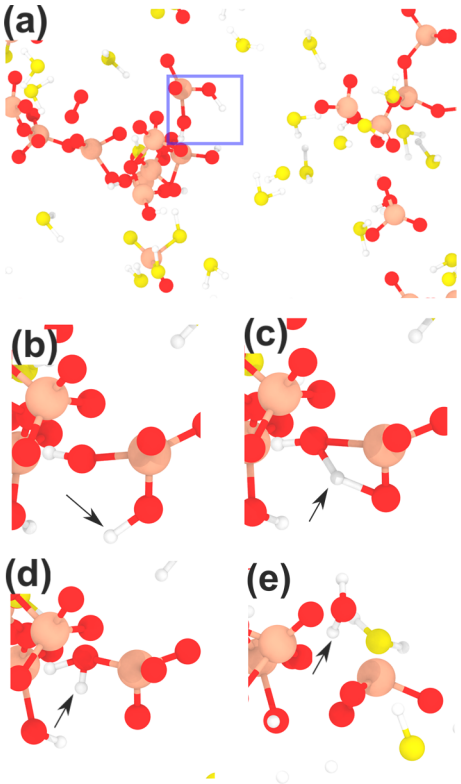

Figure 5. Reaction pathways for the subsequent H transfer between two hydroxyl groups on the oxyhydride cluster: (a) overall system snapshot at 7.48 ps. (b–e) The inset images in the blue solid rectangle in (a); (b) at 7.48; (c) at 7.49 ps; (d) at 7.51 ps; and (e) at 7.67 ps. Black arrows in (b–e) point to the H atom participating in H transfer between two hydroxyl groups, leading to the formation of a water molecule.

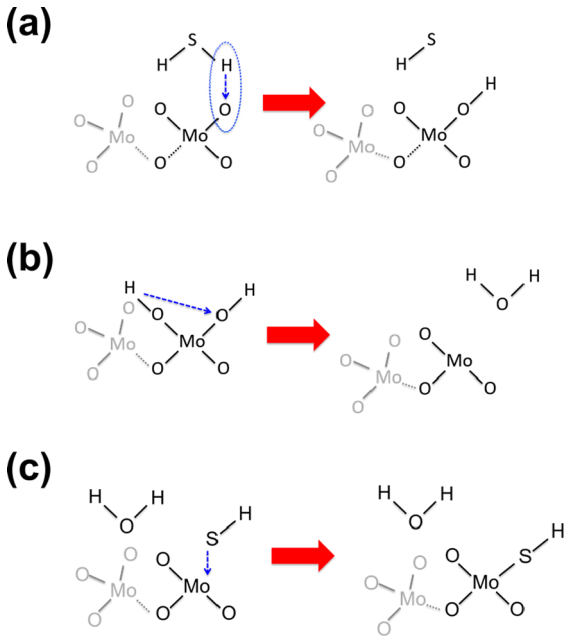

Figure 6. Schematics of reaction pathways as discussed in eqs 1 and 2: (a) H transfer from H_2S to the Mo_2O_7 cluster; (b) H transfer between two hydroxides on the same $MoO_2(OH)_2$ cluster, resulting in the formation of water and an additional O-vacancy site on the remaining Mo_xO_y cluster; (c) HS is bound to the MoO_3 cluster. Blue dotted arrows point to the key reaction steps during the QMD simulations.

coordination in the MoO_3 flake to four-fold tetrahedral coordination in transient MoO_4 clusters and Mo_2O_7 fragments. Subsequent reduction processes reduce this further to three-fold coordination (Figure 2c). Figure S1 and Table S1 depict a snapshot of the transient MoO_4 cluster and its structural characteristics, respectively, showing that one of the oxygen atoms (O4) in the cluster is only weakly bonded to the remaining MoO_3 fragment. In addition, the migration of the Mo_2O_7 cluster is fully derived by unbiased QMD simulations (i.e., not because of high pressures), as confirmed in Figure S2. We observe the following key reaction events: (1) H_2O formation (Figure 2d) and (2) Mo–S bond formation (Figure 2e). We track these reaction events and thus the overall rate of MoO_3 sulfidation by analyzing the time evolution of Mo–O and Mo–S bond populations in the system (Figure 3a). Similarly, the rate of hydrogen transfer can be tracked by plotting the number of H_2S and OH species in the simulation cell (Figure 3b).

The femtosecond time resolutions and atomistic spatial resolution of QMD simulations also allow us to monitor mechanisms for the two fundamental reaction steps, namely, hydrogen transfer from H_2S to Mo_xO_y and formation of Mo–S bonds. Figure 4a shows the overall QMD snapshot at 1.970 ps, at the beginning of H transfer and the Mo–S bond that follow.

The H transfer reaction includes the following steps: (1) A H_2S molecule diffuses close to a $Mo_xO_{y\,(x=2,3)}$ clusters (Figure 4b); (2) the cleavage of one of the H–S bonds in H_2S is accompanied by the simultaneous formation of O–H bonds between the cleaved H and the Mo_2O_7 cluster (Figure 4c); (3) the HS fragment is free to participate in a reaction with an oxygen-deficient (i.e., reduced) Mo_xO_y cluster (such as Mo_2O_6) to form the Mo–S bond (Figure 4d). These two steps can be summarized in the following reaction.

$$Mo_2O_7 + H_2S \rightarrow Mo_2O_6(OH) + HS \quad (1)$$

$$Mo_2O_6 + HS \rightarrow Mo_2O_6(SH) \quad (2)$$

The formation of the reduced Mo_xO_y cluster will be described in detail in the next section.

Movie S1 in the Supporting Information provides full dynamics of the first H transfer and Mo–S bond formation by the QMD simulations.

The formation of reduced Mo_xO_y clusters required for the sulfidation reaction occurs by the self-reduction of oxygen-rich clusters like Mo_2O_7 (see Figure 5a–e). Specifically, the transfer of multiple H atoms to the same Mo_2O_7 clusters can lead to the formation of Mo oxyhydride clusters with neighboring hydroxyl groups (Figure 5b). H atoms from one of the OH groups can preferentially react with the O atoms of the neighboring OH group to form an OH_2 group (Figure 5c,d). The strengthening of the O–H bond is accompanied by simultaneous weakening and lengthening of the Mo–O bond until the H_2O molecule is liberated (Figure 5e), leading to the formation of an effective O vacancy in the Mo_2O_7 cluster that serves as the site for nucleophilic attack by HS fragments and formation of Mo–S bonds, as described in eqs 1 and 2.

Equation 3 describes the reaction pathway for the subsequent H transfer and H_2O formation

$$Mo_2O_5(OH)_2 \rightarrow Mo_2O_6 + H_2O \quad (3)$$

Movie S2 in the Supporting Information provides full dynamics of the subsequent H transfer and water formation by the QMD simulations.

DOI: 10.1021/acs.jpclett.8b02151
J. Phys. Chem. Lett. 2018, 9, 6517–6523

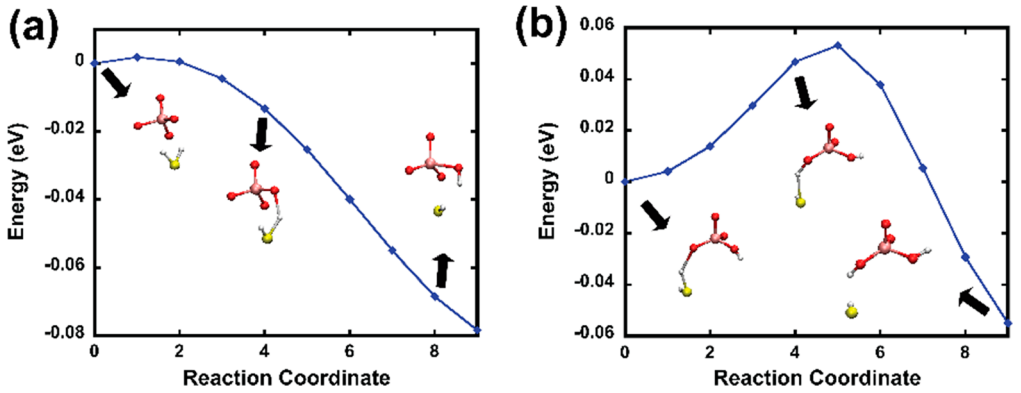

Figure 7. QMD-NEB calculations for (a) the first H transfer from the H_2S molecule to the transient MoO_4 cluster and (b) the second H atom transfer from the another H_2S molecule to the $MoO_3(OH)$ cluster, leading to the intermediate $Mo_2(OH)_2$ cluster (pink: Mo atoms; yellow: S atoms; red: O atoms; white: H atoms).

Figure 6a–c clearly summarizes the reaction pathways for H transfer and water formation as well as stable Mo–S bond formation, as shown in Figures 4 and 5. It is obvious that H transfer plays a major role in the reduction of the Mo_2O_7 cluster that leads to the formation of water and a stable Mo–S bond during the sufidation process. Namely, the H_2S molecules make $Mo_xO_{y\,(x=2,3)}$ clusters lower oxidation states, thus activating the sulfidation processes.

The reaction mechanisms in Figure 6a–c are qualitatively consistent with experimental reaction pathways such as ($MoO_3 + H_2S \rightarrow MoO_2S + H_2O$).[44] Our QMD results support experimental work that concluded that H_2S precursors to the CVD process could result in high-quality MoS_2 layers because we have confirmed that the H_2S molecule acts as an effective reducing agent for the MoO_3 flake. In addition to the sublimated Mo_xO_y fragments and water molecules, the simulation cell also contains H atoms and HS fragments formed by thermal decomposition of the H_2S precursor. Further, toward the end of our simulation trajectory, we also notice the evolution of an O_2 molecule by the self-reduction of one of the larger Mo_xO_y clusters (Figure 2d). While surprising in the overall reducing environment of the simulation cell, this observation is consistent with our previous reactive MD simulations,[35,45] as well as previous X-ray photoemission spectroscopy experiments.[27,46] To further support our proposed reaction mechanisms, we performed nudged elastic band (NEB)[47] calculations for H atom-involved reactions, leading to the formation of hydroxyl groups on the transient MoO_4 cluster. As shown in Figure 7a,b, H atom transfer from H_2S molecules to the transient MoO_4 cluster at elevated temperatures can preferably occur because of their exothermicity along with moderate reaction barriers (0.06 eV), suggesting that sulfidation of the MoO_3 flake using H_2S precursors at elevated temperatures is a thermodynamically and kinetically favorable reaction. Lastly, we calculated the Mulliken charge state of all atomic species (i.e., Mo, O, S, H) in the simulation cell as a function of time (Figure S3). Over the course of the $MoO_3 + H_2S$ reaction, Mo ions undergo strong reduction (going from the nominal +6 charge state in MoO_3 to the +4 charge state in MoS_2, consistent with prior XPS studies by Niemantsverdriet[48]). Similarly, oxygen ions are reduced, and sulfur ions undergo oxidation. XPS techniques, which are very sensitive to such variations in charge state, can be used to validate this mechanism.

In summary, we have performed QMD simulations to identify reaction pathways for the gas-phase sulfidation process of the MoO_3 flake using H_2S. The sulfidation reaction proceeds via (1) H transfer from H_2S to the Mo_2O_7 cluster leading to the formation of the Mo oxyhydrides; (2) subsequent H transfers between two hydroxyl groups on the oxyhydride cluster resulting in self-reduction and the evolution of a water molecule, thus reducing the $Mo_2O_5(OH)_2$ to Mo_2O_6; and (3) nucleophilic attack of the HS^- ligand on the reduced MoO_3 cluster forming a stable Mo–S bond. These mechanisms, fully derived by our QMD simulations, elucidate the detailed role of H transfer during the sulfidation process for CVD synthesis of MoS_2 layers. Our work provides a fundamental understanding of the atomistic reaction pathways for the sulfidation of MoO_3 assisted by H_2S. We believe that these new chemical insights will help refine reactive force fields (ReaxFF) for multimillion-atom reactive MD simulations of these systems in the same temperature range as experimental synthesis.

■ ASSOCIATED CONTENT

Supporting Information

The Supporting Information is available free of charge on the ACS Publications website at DOI: 10.1021/acs.jpclett.8b02151.

Transient MoO_4 cluster that forms a Mo_2O_7 cluster during QMD simulations, system pressures vs times during QMD simulations, and changes in atomic charges of elements during QMD simulations (PDF)

QMD trajectories describing the initial sulfidation process corresponding to Figure 4 (MP4)

QMD trajectories depicting the subsequent reaction pathway corresponding to Figure 5 (MP4).

■ AUTHOR INFORMATION

Corresponding Author

*E-mail: priyav@usc.edu.

ORCID

Sungwook Hong: 0000-0003-3569-7701
Aravind Krishnamoorthy: 0000-0001-6778-2471
Aiichiro Nakano: 0000-0003-3228-3896
Priya Vashishta: 0000-0003-4683-429X

Author Contributions

⊥C.S. and S.H. contributed equally to this work.

DOI: 10.1021/acs.jpclett.8b02151
J. Phys. Chem. Lett. 2018, 9, 6517–6523

Notes

The authors declare no competing financial interest.

■ ACKNOWLEDGMENTS

This work was supported as part of the Computational Materials Sciences Program funded by the U.S. Department of Energy, Office of Science, and Basic Energy Sciences, under Award Number DE-SC0014607. The simulations were performed at the Argonne Leadership Computing Facility under the DOE INCITE program and at the Center for High Performance Computing of the University of Southern California.

■ REFERENCES

(1) Geim, A. K.; Grigorieva, I. V. Van der Waals Heterostructures. *Nature* **2013**, *499*, 419−425.
(2) Ashton, M.; Paul, J.; Sinnott, S. B.; Hennig, R. G. Topology-Scaling Identification of Layered Solids and Stable Exfoliated 2D Materials. *Phys. Rev. Lett.* **2017**, *118*, 106101.
(3) Qin, Z.; Buehler, M. J. Nonlinear Viscous Water at Nanoporous Two-Dimensional Interfaces Resists High-Speed Flow through Cooperativity. *Nano Lett.* **2015**, *15*, 3939−44.
(4) Son, Y.-W.; Cohen, M. L.; Louie, S. G. Energy Gaps in Graphene Nanoribbons. *Phys. Rev. Lett.* **2006**, *97*, 216803.
(5) Chen, Y.; Egan, G. C.; Wan, J.; Zhu, S.; Jacob, R. J.; Zhou, W.; Dai, J.; Wang, Y.; Danner, V. A.; Yao, Y.; Fu, K.; Wang, Y.; Bao, W.; Li, T.; Zachariah, M. R.; Hu, L. Ultra-Fast Self-Assembly and Stabilization of Reactive Nanoparticles in Reduced Graphene Oxide Films. *Nat. Commun.* **2016**, *7*, 12332.
(6) Nguyen, H.; Huang, C. F.; Luo, W. J.; Xia, G. R.; Chen, Z. Q.; Li, Z. Q.; Raymond, C.; Doyle, D.; Zhao, F. Synthesis of Large-Scale 2D MoS_2 Atomic Layers by Hydrogen-Free and Promoter-Free Chemical Vapor Deposition. *Mater. Lett.* **2016**, *168*, 1−4.
(7) Tsai, M. L.; Su, S. H.; Chang, J. K.; Tsai, D. S.; Chen, C. H.; Wu, C. I.; Li, L. J.; Chen, L. J.; He, J. H. Monolayer MoS_2 Heterojunction Solar Cells. *ACS Nano* **2014**, *8*, 8317−8322.
(8) Krasnozhon, D.; Lembke, D.; Nyffeler, C.; Leblebici, Y.; Kis, A. MoS_2 Transistors Operating at Gigahertz Frequencies. *Nano Lett.* **2014**, *14*, 5905−5911.
(9) Radisavljevic, B.; Radenovic, A.; Brivio, J.; Giacometti, V.; Kis, A. Single-Layer MoS_2 Transistors. *Nat. Nanotechnol.* **2011**, *6*, 147−150.
(10) Lopez-Sanchez, O.; Lembke, D.; Kayci, M.; Radenovic, A.; Kis, A. Ultrasensitive Photodetectors Based on Monolayer MoS_2. *Nat. Nanotechnol.* **2013**, *8*, 497−501.
(11) Kaplan, D.; Gong, Y.; Mills, K.; Swaminathan, V.; Ajayan, P. M.; Shirodkar, S.; Kaxiras, E. Excitation Intensity Dependence of Photoluminescence from Monolayers of MoS_2 and WS_2/MoS_2 Heterostructures. *2D Mater.* **2016**, *3*, 015005.
(12) Mortazavi, B.; Ostadhossein, A.; Rabczuk, T.; van Duin, A. C. Mechanical Response of All-MoS_2 Single-layer Heterostructures: A ReaxFF Investigation. *Phys. Chem. Chem. Phys.* **2016**, *18*, 23695−23701.
(13) Dumcenco, D.; Ovchinnikov, D.; Lopez Sanchez, O.; Gillet, P.; Alexander, D. T. L.; Lazar, S.; Radenovic, A.; Kis, A. Large-Area MoS_2 Grown Using H_2S As the Sulphur Source. *2D Mater.* **2015**, *2*, 044005.
(14) Liu, Z.; Amani, M.; Najmaei, S.; Xu, Q.; Zou, X.; Zhou, W.; Yu, T.; Qiu, C.; Birdwell, A. G.; Crowne, F. J.; Vajtai, R.; Yakobson, B. I.; Xia, Z.; Dubey, M.; Ajayan, P. M.; Lou, J. Strain and Structure Heterogeneity in MoS_2 Atomic Layers Grown by Chemical Vapour Deposition. *Nat. Commun.* **2014**, *5*, 5246.
(15) Kim, Y.; Bark, H.; Ryu, G. H.; Lee, Z.; Lee, C. Wafer-Scale Monolayer MoS_2 Grown by Chemical Vapor Deposition Using a Reaction of MoO_3 and H_2S. *J. Phys.: Condens. Matter* **2016**, *28*, 184002.
(16) Rawal, T. B.; Le, D.; Rahman, T. S. MoS_2-Supported Gold Nanoparticle for CO Hydrogenation. *J. Phys.: Condens. Matter* **2017**, *29*, 415201.
(17) Li, H.; Du, M.; Mleczko, M. J.; Koh, A. L.; Nishi, Y.; Pop, E.; Bard, A. J.; Zheng, X. Kinetic Study of Hydrogen Evolution Reaction Over Strained MoS_2 with Sulfur Vacancies using Scanning Electrochemical Microscopy. *J. Am. Chem. Soc.* **2016**, *138*, 5123−5129.
(18) Magda, G. Z.; Peto, J.; Dobrik, G.; Hwang, C.; Biro, L. P.; Tapaszto, L. Exfoliation of Large-Area Transition Metal Chalcogenide Single Layers. *Sci. Rep.* **2015**, *5*, 14714.
(19) Muratore, C.; Hu, J. J.; Wang, B.; Haque, M. A.; Bultman, J. E.; Jespersen, M. L.; Shamberger, P. J.; McConney, M. E.; Naguy, R. D.; Voevodin, A. A. Continuous Ultra-Thin MoS_2 Films Grown by Low-Temperature Physical Vapor Deposition. *Appl. Phys. Lett.* **2014**, *104*, 261604.
(20) Venkata Subbaiah, Y.; Saji, K.; Tiwari, A. Atomically Thin MoS_2: A Versatile Nongraphene 2D Material. *Adv. Funct. Mater.* **2016**, *26*, 2046−2069.
(21) Perea-Lopez, N.; Lin, Z.; Pradhan, N. R.; Iniguez-Rabago, A.; Elias, A. L.; McCreary, A.; Lou, J.; Ajayan, P. M.; Terrones, H.; Balicas, L.; Terrones, M. CVD-Grown Monolayered MoS_2 as an Effective Photosensor Operating at Low-Voltage. *2D Mater.* **2014**, *1*, 011004.
(22) Hansen, L. P.; Johnson, E.; Brorson, M.; Helveg, S. Growth Mechanism for Single- and Multi-Layer MoS_2 Nanocrystals. *J. Phys. Chem. C* **2014**, *118*, 22768−22773.
(23) Zhan, Y.; Liu, Z.; Najmaei, S.; Ajayan, P. M.; Lou, J. Large-area Vapor-Phase Growth and Characterization of MoS_2 Atomic Layers on a SiO_2 Substrate. *Small* **2012**, *8*, 966−971.
(24) Samad, L.; Bladow, S. M.; Ding, Q.; Zhuo, J.; Jacobberger, R. M.; Arnold, M. S.; Jin, S. Layer-Controlled Chemical Vapor Deposition Growth of MoS_2 Vertical Heterostructures via van der Waals Epitaxy. *ACS Nano* **2016**, *10*, 7039−7046.
(25) Lee, Y. H.; Zhang, X. Q.; Zhang, W.; Chang, M. T.; Lin, C. T.; Chang, K. D.; Yu, Y. C.; Wang, J. T.; Chang, C. S.; Li, L. J.; Lin, T. W. Synthesis of Large-Area MoS_2 Atomic Layers with Chemical Vapor Deposition. *Adv. Mater.* **2012**, *24*, 2320.
(26) Li, H.; Wu, H.; Yuan, S.; Qian, H. Synthesis and Characterization of Vertically Standing MoS_2 Nanosheets. *Sci. Rep.* **2016**, *6*, 21171.
(27) Weber, T.; Muijsers, J. C.; vanWolput, H. J. M. C.; Verhagen, C. P. J.; Niemantsverdriet, J. W. Basic Reaction Steps in the Sulfidation of Crystalline MoO_3 to MoS_2 As Studied by X-ray Photoelectron and Infrared Emission Spectroscopy. *J. Phys. Chem.* **1996**, *100*, 14144−14150.
(28) Wei, X. M.; Zeng, H. C. Sulfidation of Single Molecular Sheets of MoO_3 Pillared by Bipyridine in Nanohybrid MoO_3(4,4'-bipyridyl)$_{0.5}$. *Chem. Mater.* **2003**, *15*, 433−442.
(29) Segall, D. E.; Strachan, A.; Goddard, W. A.; Ismail-Beigi, S.; Arias, T. A. Ab Initio and Finite-Temperature Molecular Dynamics Studies of Lattice Resistance in Tantalum. *Phys. Rev. B: Condens. Matter Mater. Phys.* **2003**, DOI: 10.1103/PhysRevB.68.014104.
(30) Zheng, M.-J.; Szlufarska, I.; Morgan, D. Ab Initio Prediction of Threshold Displacement Energies in ZrC. *J. Nucl. Mater.* **2016**, *471*, 214−219.
(31) Shimojo, F.; Hattori, S.; Kalia, R. K.; Kunaseth, M.; Mou, W.; Nakano, A.; Nomura, K.; Ohmura, S.; Rajak, P.; Shimamura, K.; Vashishta, P. A Divide-Conquer-Recombine Algorithmic Paradigm for Large Spatiotemporal Quantum Molecular Dynamics Simulations. *J. Chem. Phys.* **2014**, *140*, 18A529.
(32) Blochl, P. E. Projector Augmented-Wave Method. *Phys. Rev. B: Condens. Matter Mater. Phys.* **1994**, *50*, 17953−17979.
(33) Perdew, J. P.; Burke, K.; Ernzerhof, M. Generalized Gradient Approximation Made Simple. *Phys. Rev. Lett.* **1996**, *77*, 3865−3868.
(34) Grimme, S.; Antony, J.; Ehrlich, S.; Krieg, H. A Consistent and Accurate Ab Initio Parametrization of Density Functional Dispersion Correction (DFT-D) for the 94 Elements H-Pu. *J. Chem. Phys.* **2010**, *132*, 154104.
(35) Hong, S.; Krishnamoorthy, A.; Rajak, P.; Tiwari, S.; Misawa, M.; Shimojo, F.; Kalia, R. K.; Nakano, A.; Vashishta, P. Computational Synthesis of MoS_2 Layers by Reactive Molecular Dynamics

DOI: 10.1021/acs.jpclett.8b02151
J. Phys. Chem. Lett. 2018, 9, 6517−6523

Simulations: Initial Sulfidation of MoO_3 Surfaces. *Nano Lett.* **2017**, *17*, 4866−4872.
(36) Hardcastle, F. D.; Wachs, I. E. Determination of Molybdenum-Oxygen Bond Distances and Bond Orders by Raman Spectroscopy. *J. Raman Spectrosc.* **1990**, *21*, 683−691.
(37) Bart, J. C. J.; Ragaini, V. Molybdenum-Sulphur Bond-Strength Bond-Length Relationships. *Phosphorus Sulfur Relat. Elem.* **1980**, *8*, 161−169.
(38) Lindquist, B. A.; Takeshita, T. Y.; Woon, D. E.; Dunning, T. H., Jr. Bonding in Sulfur-Oxygen Compounds-HSO/SOH and SOO/OSO: An Example of Recoupled Pair pi Bonding. *J. Chem. Theory Comput.* **2013**, *9*, 4444−4452.
(39) Chen, J.; Tang, W.; Tian, B.; Liu, B.; Zhao, X.; Liu, Y.; Ren, T.; Liu, W.; Geng, D.; Jeong, H. Y.; et al. Chemical Vapor Deposition of High-Quality Large-Sized MoS_2 Crystals on Silicon Dioxide Substrates. *Adv. Sci.* **2016**, *3*, 1500033.
(40) Sun, L.; Leong, W. S.; Yang, S.; Chisholm, M. F.; Liang, S. J.; Ang, L. K.; Tang, Y.; Mao, Y.; Kong, J.; Yang, H. Y. Concurrent Synthesis of High-Performance Monolayer Transition Metal Disulfides. *Adv. Funct. Mater.* **2017**, *27*, 1605896.
(41) Pfrommer, B. G.; Côté, M.; Louie, S. G.; Cohen, M. L. Relaxation of Crystals with the Quasi-Newton Method. *J. Comput. Phys.* **1997**, *131*, 233−240.
(42) Nosé, S. A Unified Formulation of the Constant Temperature Molecular Dynamics Methods. *J. Chem. Phys.* **1984**, *81*, 511−519.
(43) Hoover, W. G. Canonical Dynamics: Equilibrium Phase-Space Distributions. *Phys. Rev. A: At., Mol., Opt. Phys.* **1985**, *31*, 1695.
(44) Kumar, P.; Singh, M.; Sharma, R. K.; Reddy, G. Reaction Mechanism of Core−Shell MoO_2/MoS_2 Nanoflakes via Plasma-Assisted Sulfurization of MoO_3. *Mater. Res. Express* **2016**, *3*, 055021.
(45) Hong, S.; Sheng, C.; Krishnamoorthy, A.; Rajak, P.; Tiwari, S. C.; Nomura, K.-i.; Misawa, M.; Shimojo, F.; Kalia, R. K.; Nakano, A.; et al. Chemical Vapor Deposition Synthesis of MoS_2 Layers from the Direct Sulfidation of MoO_3 Surfaces Using Reactive Molecular Dynamics Simulations. *J. Phys. Chem. C* **2018**, *122*, 7494−7503.
(46) Salazar, N.; Beinik, I.; Lauritsen, J. V. Single-Layer MoS_2 Formation by Sulfidation of Molybdenum Oxides in Different Oxidation States on Au (111). *Phys. Chem. Chem. Phys.* **2017**, *19*, 14020−14029.
(47) Henkelman, G.; Uberuaga, B. P.; Jónsson, H. A Climbing Image Nudged Elastic Band Method for Finding Saddle Points and Minimum Energy Paths. *J. Chem. Phys.* **2000**, *113*, 9901−9904.
(48) Niemantsverdriet, J. W. Case Studies in Catalyst Characterization. *Spectroscopy in Catalysis: An Introduction*; Wiley-VCH Verlag GmbH & Co.: Weinheim, Germany, 2007; pp 251−295.

DOI: 10.1021/acs.jpclett.8b02151
J. Phys. Chem. Lett. 2018, 9, 6517−6523